Progress In Electromagnetics Research B, Vol. 51, 1–32, 2013

SEASONAL DISTRIBUTION MODELING AND MAPPING OF THE EFFECTIVE EARTH RADIUS FACTOR FOR MICROWAVE LINK DESIGN IN SOUTH AFRICA

Abraham M. Nyete* **and Thomas J. O. Afullo**

Department of Electrical, Electronic and Computer Engineering, University of KwaZulu-Natal, Durban, South Africa

Abstract—In this paper we present seasonal results of the effective earth radius factor distribution in South Africa using recently (2007–2009) acquired radiosonde data from the South African Weather Service (SAWS) for seven locations in South Africa. Two data modeling methods are used to formulate the solution for the distribution of the effective earth radius factor. The seasonal effective earth radius factor statistics obtained from the radiosonde measurements are then interpolated, gridded and presented in contour maps to cover the rest of the country for the four seasons defined by ITU-R recommendation P.453-10. The Integral of Square Error is used to check the performance of the data modeling techniques while the Root Mean Square Error is used to compare the performance of the different interpolation methods used.

1. INTRODUCTION

1.1. Radio Refractivity and the Effective Earth Radius Factor (k-factor)

The vertical profile of the radio refractivity is defined in terms of the atmospheric parameters of pressure, humidity and temperature and is given by [1–8]:

$$N = \frac{77.6}{T}P + 3.3 \times 10^5 \frac{e}{T^2} \tag{1}$$

where P is the atmospheric pressure (hPa), e is the water vapour pressure (hPa), and T is the absolute temperature (K). Equation (1) is valid for radio frequencies up to 100 GHz with errors of less than

Received 4 March 2013, Accepted 11 April 2013, Scheduled 17 April 2013

* Corresponding author: Abraham M. Nyete (212536330@stu.ukzn.ac.za).

0.5% [9, 10]. From Equation (1), we see that the radio refractivity consists of a dry and wet part [9–12]:

$$N_{dry} = \frac{77.6}{T} P \tag{2}$$

and,

$$N_{wet} = 3.3 \times 10^5 \frac{e}{T^2} \tag{3}$$

If the radio refractivity varies linearly with height h for the first few tenths of a kilometer above the earth's surface and doesn't vary in the horizontal direction, then the vertical refractivity gradient is given by [13–15]:

$$\frac{dN}{dh} = 77.6 \left(\frac{1}{T} \frac{dP}{dh} + \frac{4810}{T^2} \frac{de}{dh} \right) \tag{4}$$

Electromagnetic waves travelling through the atmosphere are usually bent due to radio refractivity. For ease of geometrical analysis, these waves are represented as straight lines then compensation is done by assuming an imaginary earth radius, otherwise referred to as effective earth radius, r_e [15]. The ratio between the effective and true earth radius is referred to as the effective earth radius factor (k-factor) and is given by [10, 16, 17]:

$$k = \frac{r_e}{r_o} = 1 + r_o \frac{dn}{dh} \tag{5}$$

where k is the effective earth radius factor and r_e is the effective earth radius and r_o is the true earth radius and $\frac{dn}{dh}$ is the refractive index gradient. The k-factor is a function of the vertical refractivity gradient, dN/dh, and can also be determined from [13, 15, 18]:

$$k = \left[1 + \frac{dN/dh}{157} \right]^{-1} \tag{6}$$

1.2. Diffraction (k-factor) Fading

When a radio wave travelling from the transmitting antenna to the receiving antenna is intercepted by an obstacle, the signal is diffracted and consequently fading occurs. This type of fading occurs when the signal encounters either a single or multiple obstacles along its path. If the choice of both the median and effective values of the effective earth radius factor for link design is not appropriate for the particular topographical setting, the signal may be obstructed by the Earth and consequently little or no signal is detected at the receiver. This scenario

is common when the k-factor assumes very low values (sub-refraction) and hence the need to determine the appropriate minimum k-factor for any particular link application [19]. This is the commonly referred to as the k-factor exceeded 99.9% of the time (effective k-factor) value. Both the median and effective values of the k-factor are essential in the determination of the appropriate antenna heights necessary to achieve adequate path clearance for the particular link application. ITU-R recommendation P.530-14 [20] outlines the procedure for the determination of appropriate antenna heights to avoid over or under estimations that could lead to unnecessarily long or short antennas. The procedures outlined in this recommendation underscore the need for appropriate determination of the accurate values of the k-factor for link design applications whenever local data is available. This procedure is key to avoiding wastage of resources in expensive re-designs and loss of revenue incase outage is experienced for example in Global System for Mobile communications (GSM), Universal Mobile Telecommunications System (UMTS) and Long Term Evolution (LTE) networks which are the key modes of land mobile communications currently.

1.3. Previous Work on the Effective Earth Radius Factor in Africa

Various reports have been presented on the refractivity and k-factor for Nigeria. The authors have worked on refractivity and k-factor statistics for various locations across the country using measurements from meteorological sensors either mounted on TV towers or ground measurements [2, 3, 5, 10, 18]. Palmer and Baker [13–15] have used regression analysis on data for summer inland rainfall areas of South Africa to develop a cumulative distribution model of the k-factor. Using this model they were also able to obtain contours of the k-factor exceeded 0.001 of the time annually. Odedin and Afullo [19, 21, 22] have also worked on the seasonal and annual k-factor variations and models for Durban in South Africa and Maun in Botswana. They have been able to develop curve fitting models of the k-factor for Durban and curve fitting and kernel models of the k-factor for Maun Botswana using eight months and three years data respectively. Most recently Fulgence [23] has worked on k-factor statistics for Central Africa, particularly Rwanda and North-Western Tanzania for seven locations. He was able to obtain the doubly truncated and kernel models of the k-factor for the seven locations studied. He also extended the k-factor statistics to cover the rest of the region by using kriging implementation in ArcGIS to produce contours of the k-factor not exceeded for 0.5 of the time.

2. DISTRIBUTION MODELING

Two different methods of modeling the seasonal k-factor statistics for South Africa have been applied. These are the kernel and the curve-fitting methods.

2.1. Curve-fitting Method

The curve-fitting method used here is based on an algorithm developed by Odedin and Afullo [19, 21] for modeling the probability density function (pdf) of the k-factor. A Gaussian distribution of the measured data is assumed and then the parameters A, $\propto$, and μ_k, as defined in [19, 21] are computed. The pdf model used has the following basic form [19, 21]:

$$f(k) = Ae^{-\propto(k-\mu_k)^2} \tag{7}$$

ITU-R Recommendation P.453-12 [11] contains world refractivity gradient maps for the months of February, May, August and November but recommends that where local reliable data is available, the same should be determined. Using three years (2007–2009) recent meteorological radiosonde measurements obtained from the South African Weather Service (SAWS), k-factor curve-fitting models for the four months (seasons) of the year recommended in [11], that is; February, May, August and November have been formulated for the seven locations studied at a height of 200 m above ground level.

2.1.1. Curve-fitting Results and Discussion

Figures 1–28 show the seasonal curve-fitting model plots of the k-factor distribution for the seven locations where measurements were taken. Table 1 shows the values of the parameters obtained both from

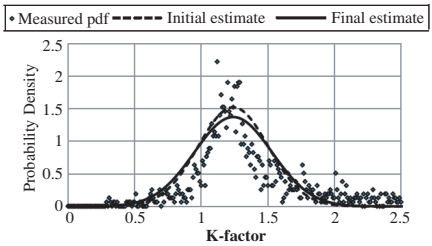

Figure 1. Gaussian curve-fitting estimate, Bloemfontein, February, 200 m a.g.l.

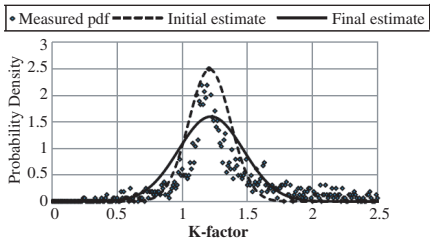

Figure 2. Gaussian curve-fitting estimate, Bloemfontein, May, 200 m a.g.l.

Table 1. Seasonal curve-fitting values of A, u_k and ISE.

Station	**Initial estimates from measurements**				**Final estimates from curve-fitting**		
	Month	$\mathbf{u_k}$	**A**	**ISE**	$\mathbf{u_k}$	**A**	**ISE**
Bloemfontein	Feb.	1.24	1.52	0.188	1.24	1.37	0.184
	May	1.21	2.49	0.338	1.22	1.6	0.244
	Aug.	1.21	2.7	0.425	1.21	1.79	0.334
	Nov.	1.22	1.87	0.275	1.25	1.30	0.220
Cape Town	Feb.	1.26	1.17	0.105	1.27	1.16	0.104
	May	1.29	2.11	0.209	1.29	1.45	0.133
	Aug.	1.3	1.63	0.157	1.29	1.7	0.156
	Nov	1.27	1.45	0.1153	1.27	1.48	0.115
Durban	Feb.	1.28	1.24	0.099	1.26	1.37	0.091
	May	1.26	1.45	0.133	1.26	1.37	0.131
	Aug.	1.26	1.51	0.141	1.25	1.64	0.137
	Nov.	1.26	1.54	0.102	1.26	1.66	0.098
Polokwane	Feb.	1.27	2.32	0.228	1.24	1.66	0.124
	May	1.27	1.26	0.20	1.24	1.55	0.174
	Aug.	1.23	1.96	0.185	1.21	2.08	0.174
	Nov.	1.23	2	0.191	1.21	1.79	0.178
Pretoria	Feb.	1.22	1.29	0.122	1.20	1.5	0.109
	May	1.19	2.39	0.165	1.18	2.2	0.157
	Aug.	1.19	3.01	0.258	1.17	2.45	0.209
	Nov.	1.20	1.75	0.123	1.20	1.79	0.122
Upington	Feb.	1.14	1.63	0.152	1.13	1.46	0.146
	May	1.20	1.82	0.184	1.21	1.58	0.175
	Aug.	1.19	1.6	0.224	1.19	1.59	0.223
	Nov.	1.16	1.08	0.279	1.15	1.38	0.257
Bethlehem	Feb.	1.16	2.09	0.370	1.20	2.09	0.333
	May	1.21	1.23	2.06	1.21	3.53	1.27
	Aug.	1.17	1.46	0.947	1.19	2.92	0.569
	Nov.	1.14	4.15	1.51	1.21	2.03	0.623

measurements and modeling. The initial estimate and final model integral of square errors (ISE) are also calculated as shown in Table 1. The final estimate is the best estimate since the error achieved is at the very minimum. From this table, the curve-fitting median k-factor values for Bloemfontein are found to be 1.24 for February, 1.22 for May, 1.21 for August and 1.25 for November. For Cape Town, the values are 1.27 for February, 1.29 for May, 1.29 for August and 1.27 for

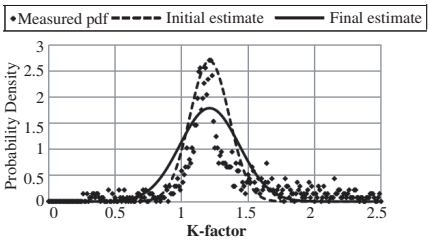

Figure 3. Gaussian curve-fitting estimate, Bloemfontein, August, 200 m a.g.l.

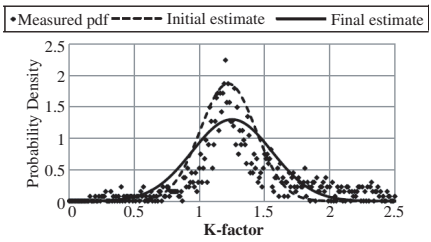

Figure 4. Gaussian curve-fitting estimate, Bloemfontein, November, 200 m a.g.l.

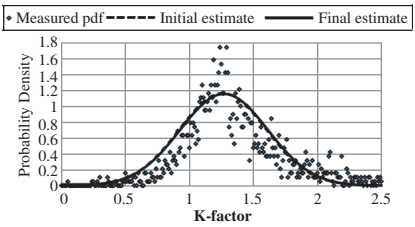

Figure 5. Gaussian curve-fitting estimate, Cape Town, February, 200 m a.g.l.

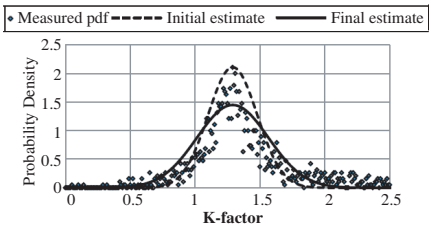

Figure 6. Gaussian curve-fitting estimate, Cape Town, May, 200 m a.g.l.

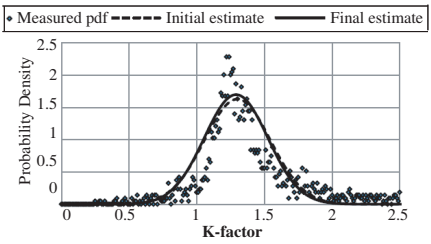

Figure 7. Gaussian curve-fitting estimate, Cape Town, August, 200 m a.g.l.

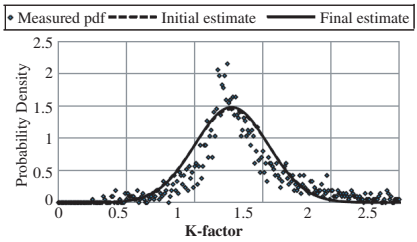

Figure 8. Gaussian curve-fitting estimate, Cape Town, November, 200 m a.g.l.

November. For Durban, the values are 1.26 for February, 1.26 for May, 1.25 for August and 1.26 for November. For Polokwane, the values are 1.24 for February, 1.24 for May, 1.21 for August and 1.21 for November. For Pretoria, the values are 1.20 for February, 1.18 for May, 1.17 for August and 1.20 for November. For Upington, the values are 1.13 for February, 1.21 for May, 1.19 for August and 1.15 for November. For Bethlehem, the values are 1.20 for February, 1.21 for May, 1.19 for

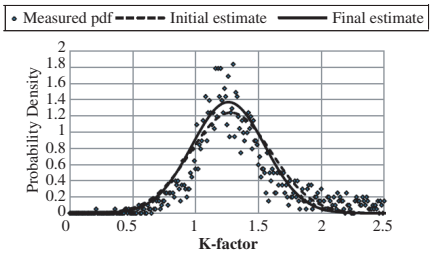

Figure 9. Gaussian curve-fitting estimate, Durban, February, 200 m a.g.l.

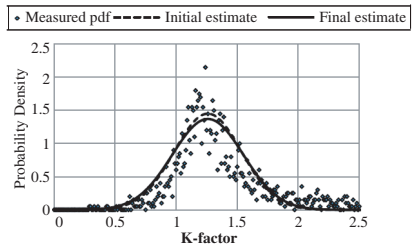

Figure 10. Gaussian curve-fitting estimate, Durban, May, 200 m a.g.l.

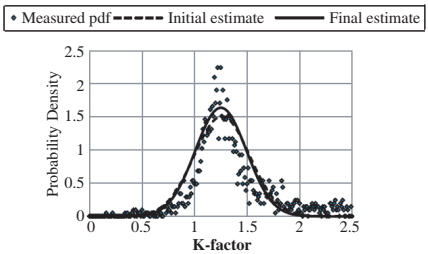

Figure 11. Gaussian curve-fitting estimate, Durban, August, 200 m a.g.l.

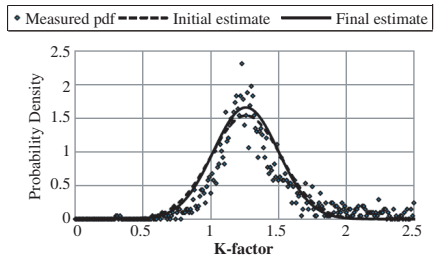

Figure 12. Gaussian curve-fitting estimate, Durban, November, 200 m a.g.l.

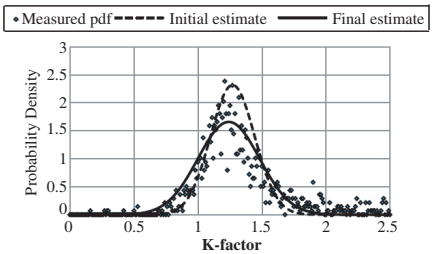

Figure 13. Gaussian curve-fitting estimate, Polokwane, February, 200 m a.g.l.

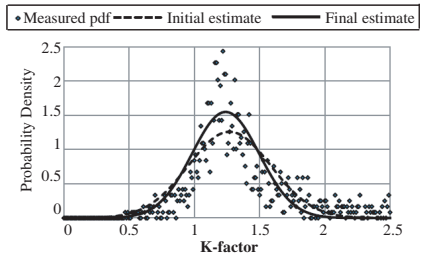

Figure 14. Gaussian curve-fitting estimate, Polokwane, May, 200 m a.g.l.

August and 1.21 for November. Also, for Bloemfontein, the largest error is found to be 0.334 for the month of August while the least error is found to be 0.184 for the month of February. For Cape Town, the largest error is 0.156 for the month of August while the least error is found to be 0.104 for the month of February. For Cape Town, the

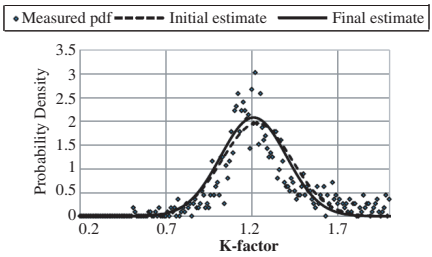

Figure 15. Gaussian curve-fitting estimate, Polokwane, August, 200 m a.g.l.

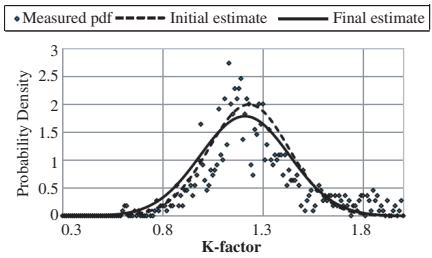

Figure 16. Gaussian curve-fitting estimate, Polokwane, November, 200 m a.g.l.

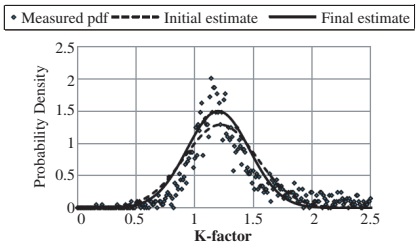

Figure 17. Gaussian curve-fitting estimate, Pretoria, February, 200 m a.g.l.

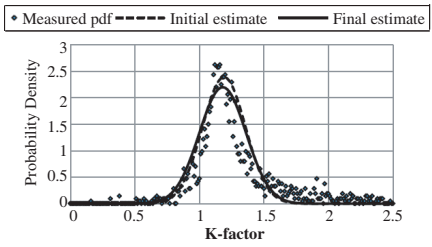

Figure 18. Gaussian curve-fitting estimate, Pretoria, May, 200 m a.g.l.

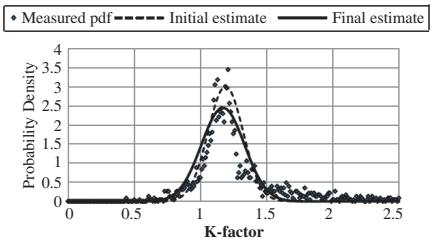

Figure 19. Gaussian curve-fitting estimate, Pretoria, August, 200 m a.g.l.

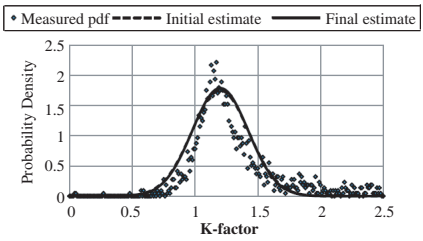

Figure 20. Gaussian curve-fitting estimate, Pretoria, November, 200 m a.g.l.

largest error is 0.156 for the month of August while the least error is found to be 0.104 for the month of February. For Durban, the largest error is 0.137 for the month of August while the least error is found to be 0.091 for the month of February. For Polokwane, the largest error is 0.178 for the month of November while the least error is found to be 0.124 for the month of February. For Pretoria, the largest error is

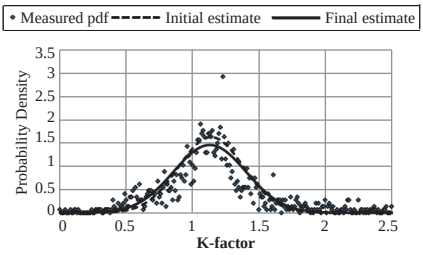

Figure 21. Gaussian curve-fitting estimate, Upington, February, 200 m a.g.l.

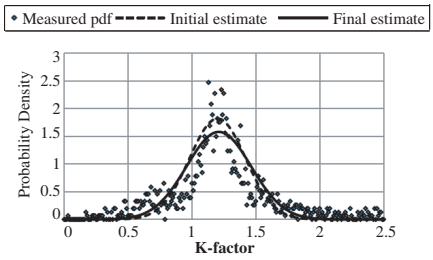

Figure 22. Gaussian curve-fitting estimate, upington, May, 200 m a.g.l.

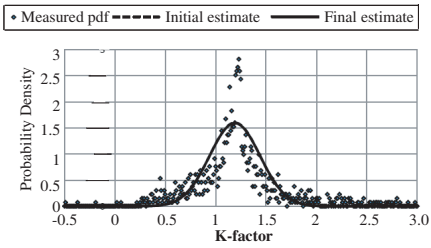

Figure 23. Gaussian curve-fitting estimate, upington, August, 200 m a.g.l.

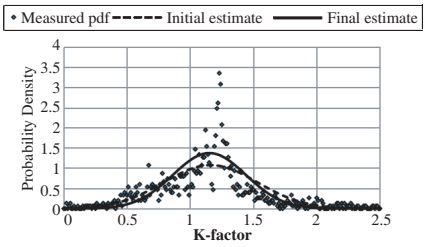

Figure 24. Gaussian curve-fitting estimate, upington, November, 200 m a.g.l.

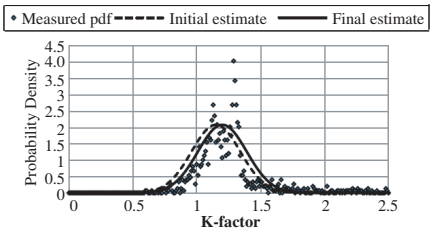

Figure 25. Gaussian curve-fitting estimate, Bethlehem, February, 200 m a.g.l.

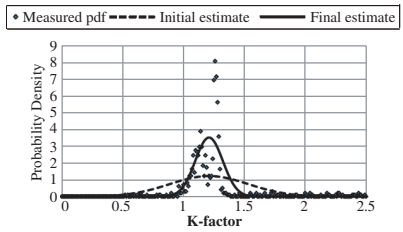

Figure 26. Gaussian curve-fitting estimate, Bethlehem, May, 200 m a.g.l.

0.209 for the month of August while the least error is found to be 0.109 for the month of February. For Upington, the largest error is 0.223 for the month of August while the least error is found to be 0.146 for the month of February. For Bethlehem, the largest error is 1.27 for the month of August while the least error is found to be 0.333 for the month of February. Table 2 shows the curve-fitting models obtained.

Table 2. Seasonal Gaussian curve-fitting k-factor distribution models.

Location	**Month**	**Distribution Model**
Bloemfontein	Feb.	$f(k) = 1.37e^{-5.9(k-1.24)^2}$
	May	$f(k) = 1.6e^{-8.04(k-1.22)^2}$
	Aug.	$f(k) = 1.79e^{-10.07(k-1.21)^2}$
	Nov.	$f(k) = 1.30e^{-5.31(k-1.25)^2}$
Cape Town	Feb.	$f(k) = 1.16e^{-4.23(k-1.27)^2}$
	May	$f(k) = 1.45e^{-6.61(k-1.29)^2}$
	Aug.	$f(k) = 1.7e^{-9.08(k-1.29)^2}$
	Nov	$f(k) = 1.48e^{-6.88(k-1.27)^2}$
Durban	Feb.	$f(k) = 1.37e^{-5.9(k-1.26)^2}$
	May	$f(k) = 1.37e^{-5.9(k-1.26)^2}$
	Aug.	$f(k) = 1.64e^{-8.45(k-1.25)^2}$
	Nov.	$f(k) = 1.66e^{-8.66(k-1.26)^2}$
Polokwane	Feb.	$f(k) = 1.66e^{-8.66(k-1.24)^2}$
	May	$f(k) = 1.55e^{-7.55(k-1.24)^2}$
	Aug.	$f(k) = 2.08e^{-13.59(k-1.21)^2}$
	Nov	$f(k) = 1.79e^{-10.07(k-1.21)^2}$
Pretoria	Feb.	$f(k) = 1.5e^{-7.07(k-1.20)^2}$
	May	$f(k) = 2.2e^{-15.21(k-1.18)^2}$
	Aug.	$f(k) = 2.45e^{-18.86(k-1.17)^2}$
	Nov.	$f(k) = 1.79e^{-10.07(k-1.20)^2}$
Upington	Feb	$f(k) = 1.46e^{-6.7(k-1.13)^2}$
	May	$f(k) = 1.58e^{-7.84(k-1.21)^2}$
	Aug.	$f(k) = 1.59e^{-7.94(k-1.19)^2}$
	Nov.	$f(k) = 1.38e^{-5.98(k-1.15)^2}$
Bethlehem	Feb.	$f(k) = 2.09e^{-13.72(k-1.20)^2}$
	May	$f(k) = 3.53e^{-39.15(k-1.21)^2}$
	Aug.	$f(k) = 2.92e^{-26.79(k-1.19)^2}$
	Nov.	$f(k) = 2.03e^{-12.95(k-1.21)^2}$

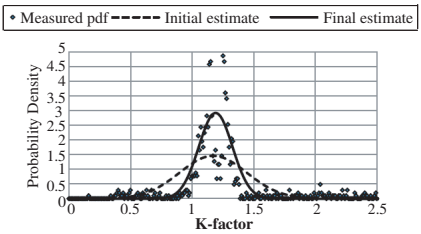

Figure 27. Gaussian curve-fitting estimate, Bethlehem, August, 200 m a.g.l.

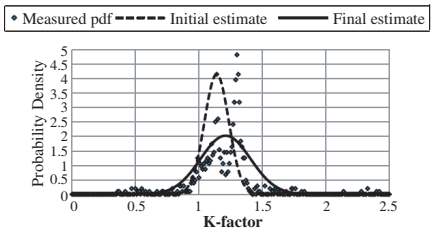

Figure 28. Gaussian curve-fitting estimate, Bethlehem, November, 200 m a.g.l.

2.2. Kernel Density Estimation

While histograms are traditionally the most common non-parametric method of representing data distribution, there are serious limitations associated with them. Some of these limitations are; that they depend on the width of the bins and their end points and also lack continuity (not smooth) [24]. Large bin sizes will result in only few regions being represented while very small bins will result in some empty bins. Kernel density estimators were introduced to deal with these challenges associated with histograms. This implies that, as with histograms, the kernel probability density function (pdf) is directly estimated from the data sample and therefore has no fixed data structure [24]. Thus, non-parametric methods avoid any restrictive assumptions about the form of the data distribution. Hence, non-parametric estimators have the advantage that they are able to reveal data structural features that parametric methods may miss out. To alleviate the dependence on bin end points experienced with histograms, kernel density estimators centre a kernel function at each data point thereby spreading the influence of each data point about its neighborhood. These kernel functions on each data point are then summed up together resulting in smooth curve. The kernel density estimate of a variable k whose kernel function is $K(k)$ is then given by [24–29]:

$$f(k) = \frac{1}{nh} \sum_{i=1}^{n} K\left(\frac{k - X_i}{n}\right) \tag{8}$$

where n is the number of samples, h the window width, and X_i the ith observation. The kernel function choice has no much influence on the final density estimate as compared to the choice of the window width, h, which determines the overall structure of the kernel density estimate. The number of data samples as well as the type of kernel function will particularly determine the optimal window width chosen for each data

application. The kernel functions, their efficiencies and formulae for calculating the optimum window width for the four kernels used in this paper are shown in Table 3 [22, 26, 27]. However, none of these plug-in formulae in Table 3 will produce the global minimum of the error and so several iterations of computing the error will always be required to achieve the best result. This window width is optimum in that the error achieved between the measured and the kernel estimate is at its minimum. As the number of data samples increases, the value of the window width decreases. The most commonly used error criteria for optimizing the window width are the integral of square error (ISE) and the mean integral of square error (MISE). They are given by [28–30]:

$$\mathrm{ISE} = \int_{-\infty}^{\infty} \left[f\left(k\right) - f^{*}(k)\right]^{2} dk \tag{9}$$

and,

$$\mathrm{MISE} = E \int_{-\infty}^{\infty} \left[f\left(k\right) - f^{*}(k)\right]^{2} dk \tag{10}$$

The ISE is the one chosen for this presentation. The kernel function is a true pdf centered at zero and it follows that the resulting kernel density estimate is also a true pdf. Therefore, kernels functions have the following properties [25–27]:

$$\int_{-\infty}^{+\infty} K(k)dk = 1 \tag{11}$$

$$\int_{-\infty}^{+\infty} kK(k)dk = 0 \tag{12}$$

$$\int_{-\infty}^{+\infty} k^{2}K(k)dk > 0 \tag{13}$$

The four kernels in Table 3 are used to model the seasonal (February, May, August and November)median k-factor (μ_k) distribution across the seven locations in South Africa using a code programmed in MATLAB.

2.2.1. Kernel Results and Discussion

Due to space considerations, only kernel models that produce the least error are plotted. The ISE error criterion is used to optimize the model solutions. Figures 29–56 show the best kernel models for each season and location. In Table 4, three values of the smoothing parameter

Table 3. Kernels, Kernel functions and their efficiencies.

Kernel	Kernel function, $K(k)$	Efficiency (%)	Optimal window width
Epanechnikov	$K(k) = \begin{cases} \frac{3}{4\sqrt{5}}\left(1-\frac{1}{5}k^2\right), -\sqrt{5} \le k \le \sqrt{5} \\ 0, \quad \& \ elsewhere \end{cases}$	100	$\frac{2.34\sigma}{n^5}$
Triangular	$K(k) = \begin{cases} \frac{15}{16}(1-k), -1 \le k \le 1 \\ 0, \quad \& \ elsewhere \end{cases}$	98.6	$\frac{2.58\sigma}{n^5}$
Gaussian	$K(k) = \frac{1}{\sqrt{2\pi}} e^{-\left(\frac{k^2}{2}\right)}, \ -\infty < k < \infty$	95.1	$\frac{1.06\sigma}{n^5}$
Rectangular	$K(k) = \begin{cases} \frac{1}{2}, -1 \le k \le 1 \\ 0, \ \& \ elsewhere \end{cases}$	93	$\frac{1.84\sigma}{n^5}$

have been presented in each case and the best choice of the smoothing parameter is the one which produces the least error. The models obtained show that the values of the smoothing parameter around the optimal value produce models that are very similar in shape and the only way to differentiate them is by comparing the errors. From Figures 29–56, the best kernel models for Bloemfontein are Rectangular for all the four seasons and the optimum window width, h, is 0.006 for all the four months. For Cape Town, the best model is Rectangular with an optimum window width of 0.006 for February and May while it is Epanechnikov with an optimum window width of 0.006 for August and November. For Durban, the best model is Rectangular with an optimum window width of 0.006 for February and August while the best for May is Triangular with an optimum window width of 0.006 and for November it is Epanechnikov with an optimum window width of 0.006. Epanechnikov kernel model with an optimum window width of 0.006 is the best for Polokwane in February and also in May with an optimum window width of 0.007 and November with an optimum window width of 0.005 while the Rectangular model with an optimum window width of 0.006 is the best for August. The Rectangular model with an optimum window width of 0.006 is the best for all the four seasons in Pretoria. For Upington, the Rectangular model with an optimum window width of 0.006 is the best for February and May while the Gaussian (with an optimum window width of 0.007) and Epanechnikov (with an optimum window width of 0.006) models are the best for August and the Epanechnikov model with an optimum window width of 0.005 is best for November. The rectangular model with an optimum window width of 0.006 is the best for all the four months in Bethlehem.

From these models the median k-factor values are obtained. For Bloemfontein the median k-factor value is 1.22 for February, 1.20 for May, 1.21 for August and 1.20 for November. For Cape Town, it is 1.23 for February, 1.29 for May, 1.29 for August and 1.26 for November. For Durban, it is 1.29 for February, 1.26 for May, 1.26 for August and 1.24 for November. For Polokwane, it is 1.25 for February, 1.26 for May, 1.23 for August and 1.22 for November. For Pretoria, it is 1.21 for February, 1.19 for May, 1.20 for August and 1.21 for November. For Upington, it is 1.15 for February, 1.21 for May, 1.18 from Epanechnikov model

Table 4. (a) Seasonal kernel median k-factor, ISE and h comparison. (b) Seasonal kernel median k-factor, ISE and h comparison. (c) Seasonal kernel median k-factor, ISE and h comparison.

(a)

Location	Month	h	Kernel							
			Gaussian		Triangular		Epanechnikov		Rectangular	
			μ_k	ISE	μ_k	ISE	μ_k	ISE	μ_k	ISE
Bloemfontein	Feb.	0.006	1.23	0.0353	1.24	0.0343	1.24	0.0324	1.22	0.0321
		0.007	1.23	0.0343	1.24	0.0345	1.24	0.0327	1.22	0.0330
		0.02	1.24	0.0453	1.25	0.0457	1.25	0.0478	1.24	0.0535
	May	0.006	1.20	0.0350	1.21	0.0336	1.20	0.0317	1.20	0.0302
		0.007	1.20	0.0332	1.21	0.0331	1.20	0.0316	1.20	0.0326
		0.008	1.20	0.0328	1.21	0.0336	1.20	0.0331	1.20	0.0349
	Aug.	0.006	1.22	0.0324	1.21	0.0313	1.22	0.0301	1.21	0.0300
		0.007	1.22	0.0313	1.21	0.0316	1.22	0.0320	1.21	0.0339
		0.02	1.20	0.0471	1.21	0.0482	1.19	0.0510	1.19	0.0572
	Nov.	0.005	1.21	0.0427	1.22	0.0408	1.21	0.0391	1.20	0.0435
		0.006	1.21	0.0405	1.22	0.0402	1.21	0.0396	1.20	0.0385
		0.02	1.19	0.0581	1.19	0.0590	1.19	0.0623	1.19	0.0683
Cape Town	Feb.	0.006	1.24	0.0263	1.24	0.0253	1.25	0.0240	1.23	0.0220
		0.007	1.24	0.0251	1.24	0.0249	1.25	0.0241	1.23	0.0250
		0.008	1.24	0.0250	1.24	0.0255	1.25	0.0251	1.23	0.0277
	May	0.006	1.30	0.0340	1.30	0.0326	1.29	0.0316	1.29	0.0304
		0.007	1.30	0.0326	1.30	0.0321	1.29	0.0311	1.29	0.0313
		0.008	1.30	0.0323	1.30	0.0326	1.29	0.0320	1.29	0.0320
	Aug.	0.005	1.28	0.0267	1.28	0.0260	1.29	0.0247	1.28	0.0254
		0.006	1.28	0.0247	1.28	0.0243	1.29	0.0236	1.28	0.0255
		0.007	1.28	0.0244	1.28	0.0253	1.29	0.0248	1.28	0.0271
	Nov.	0.006	1.25	0.0281	1.26	0.0280	1.26	0.0272	1.27	0.0277
		0.007	1.25	0.0277	1.26	0.0285	1.26	0.0285	1.27	0.0316
		0.02	1.24	0.0353	1.24	0.0355	1.25	0.0370	1.26	0.0398

(b)

Location	Month	h	Kernel							
			Gaussian		Triangular		Epanechnikov		Rectangular	
			μ_k	ISE	μ_k	ISE	μ_k	ISE	μ_k	ISE
Durban	Feb.	0.005	1.29	0.0300	1.28	0.0292	1.28	0.0284	1.29	0.0304
		0.006	1.29	0.0290	1.28	0.0293	1.28	0.0287	1.29	0.0282
		0.02	1.28	0.0361	1.26	0.0363	1.27	0.0374	1.26	0.0395
	May	0.003	1.24	0.0514	1.24	0.0496	1.24	0.0486	1.25	0.0481
		0.006	1.25	0.0340	1.26	0.0337	1.27	0.0338	1.25	0.0353
		0.04	1.23	0.0591	1.23	0.0582	1.23	0.0595	1.21	0.0602
	Aug.	0.006	1.25	0.0277	1.26	0.0273	1.25	0.0263	1.26	0.0233
		0.007	1.25	0.0268	1.26	0.0268	1.25	0.0261	1.26	0.0283
		0.02	1.23	0.0349	1.23	0.0353	1.23	0.0368	1.24	0.0401
	Nov.	0.006	1.24	0.0225	1.24	0.0222	1.24	0.0215	1.25	0.0219
		0.007	1.24	0.0223	1.24	0.0224	1.24	0.0218	1.25	0.0241
		0.02	1.25	0.0333	1.25	0.0337	1.26	0.0357	1.26	0.0392
Polokwane	Feb.	0.006	1.26	0.0470	1.26	0.0451	1.25	0.0444	1.27	0.0468
		0.007	1.26	0.0462	1.26	0.0460	1.25	0.0452	1.27	0.0460
		0.02	1.25	0.0655	1.25	0.0670	1.25	0.0707	1.25	0.0780
	May	0.006	1.27	0.0635	1.26	0.0601	1.26	0.0565	1.25	0.0487
		0.007	1.27	0.0595	1.26	0.0576	1.26	0.0548	1.25	0.0552
		0.008	1.27	0.0584	1.26	0.0584	1.26	0.0555	1.25	0.0566
	Aug.	0.006	1.22	0.0552	1.21	0.0548	1.23	0.0538	1.22	0.0532
		0.007	1.22	0.0553	1.21	0.0566	1.23	0.0564	1.22	0.0548
		0.008	1.22	0.0565	1.21	0.0587	1.23	0.0599	1.22	0.0634
	Nov.	0.005	1.23	0.0531	1.22	0.0521	1.22	0.0517	1.22	0.0552
		0.006	1.23	0.0533	1.22	0.0541	1.22	0.0548	1.22	0.0547
		0.007	1.23	0.0548	1.22	0.0567	1.22	0.0591	1.22	0.0662
Pretoria	Feb .	0.006	1.21	0.0265	1.22	0.0256	1.23	0.0245	.21	0.0228
		0.007	1.21	0.0253	1.22	0.0252	1.23	0.0244	1.21	0.0268
		0.008	1.21	0.0252	1.22	0.0256	1.23	0.0251	1.21	0.0264
	May	0.006	1.18	0.0275	1.19	0.0266	1.20	0.0255	1.19	0.0235
		0.007	1.18	0.0265	1.19	0.0265	1.20	0.0260	1.19	0.0289
		0.008	1.18	0.0264	1.19	0.0271	1.20	0.0273	1.19	0.0298
	Aug.	0.006	1.20	0.0300	1.20	0.0291	1.21	0.0279	1.20	0.0261
		0.007	1.20	0.0291	1.20	0.0290	1.21	0.0281	1.20	0.0294
		0.008	1.20	0.0290	1.20	0.0295	1.21	0.0289	1.20	0.0293
	Nov.	0.006	1.21	0.0220	1.22	0.0215	1.22	0.0207	1.21	0.0190
		0.007	1.21	0.0210	1.22	0.0211	1.22	0.0210	1.21	0.0222
		0.008	1.21	0.0209	1.22	0.0213	1.22	0.0215	1.21	0.0251

Upington	Feb.	0.005	1.14	0.0476	1.14	0.0458	1.15	0.0447	1.15	0.0467
		0.006	1.14	0.0458	1.14	0.0456	1.15	0.0448	1.15	0.0433
		0.01	1.13	0.0510	1.14	0.0522	1.15	0.0543	1.15	0.0592
	May	0.006	1.20	0.0454	1.21	0.0445	1.20	0.0418	1.21	0.0382
		0.007	1.20	0.0433	1.21	0.0435	1.20	0.0422	1.21	0.0452
		0.008	1.20	0.0428	1.21	0.0437	1.20	0.0432	1.21	0.0460
	Aug.	0.006	1.20	0.0398	1.19	0.0399	1.18	0.0393	1.18	0.0406
		0.007	1.20	0.0393	1.19	0.0400	1.18	0.0406	1.18	0.0449
		0.008	1.20	0.0398	1.19	0.0408	1.18	0.0419	1.18	0.0481
	Nov.	0.005	1.18	0.0380	1.17	0.0372	1.17	0.0357	1.16	0.0393
		0.006	1.18	0.0363	1.17	0.0367	1.17	0.0359	1.16	0.0371
		0.007	1.18	0.0361	1.17	0.0368	1.17	0.0370	1.16	0.0405

(c)

Location	Month	h	Kernel							
			Gaussian		Triangluar		Epanechnikov		Rectangular	
			μ_k	ISE	μ_k	ISE	μ_k	ISE	μ_k	ISE
Bethlehem	Feb.	0.006	1.16	0.0454	1.17	0.0442	1.18	0.0428	1.17	0.0404
		0.007	1.16	0.0450	1.17	0.0451	1.18	0.0438	1.17	0.0459
		0.04	1.19	0.1341	1.18	0.1413	1.17	0.1514	1.18	0.1675
	May	0.002	1.19	0.2313	1.19	0.2220	1.19	0.2296	1.18	0.2318
		0.006	1.20	0.1382	1.21	0.1356	1.20	0.1345	1.21	0.1332
		0.05	1.22	0.9576	1.23	0.012	1.23	1.120	1.22	0.2658
	Aug.	0.003	1.16	0.1193	1.16	0.1156	1.16	0.1176	1.15	0.1308
		0.006	1.17	0.0968	1.18	0.0960	1.18	0.0950	1.16	0.0944
		0.05	1.18	0.4128	1.19	0.4303	1.19	0.4682	1.20	0.5204
	Nov.	0.005	1.15	0.0648	1.14	0.0608	1.14	0.0599	1.15	0.0638
		0.006	1.15	0.0618	1.14	0.0614	1.14	0.0601	1.15	0.0582
		0.007	1.15	0.0613	1.14	0.0622	1.14	0.0633	1.15	0.0670

and 1.20 form Gaussian model for August and 1.17 for November.For Bethlehem, it is 1.17 for February, 1.21 for May, 1.16 for August and 1.15 for November.

3. INTERPOLATION AND MAPPING

Interpolation refers to the process of predicting data values at locations where samples are not available using data from surrounding locations within a particular geographical range (area) [31, 32]. There are two broad categories of interpolation techniques namely; global and local methods. Global methods consider all known samples to estimate the

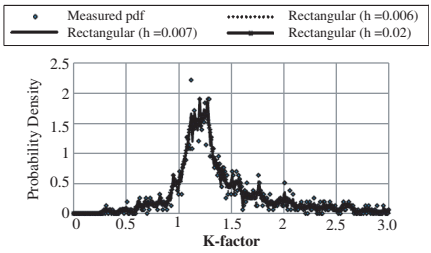

Figure 29. Rectangular kernel density estimate, Bloemfontein, February, 200 m a.g.l.

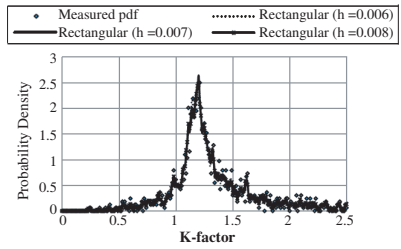

Figure 30. Rectangular kernel density estimate, Bloemfontein, May, 200 m a.g.l.

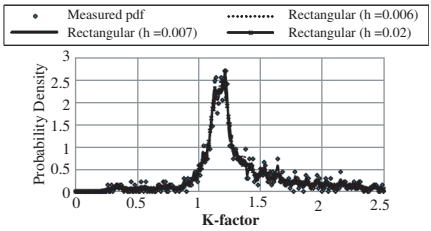

Figure 31. Rectangular kernel density estimate, Bloemfontein, August, 200 m a.g.l.

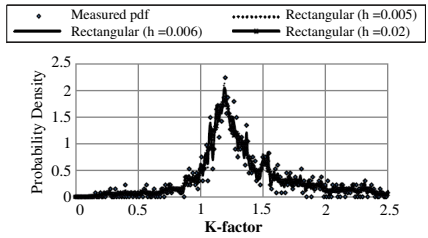

Figure 32. Rectangular kernel density estimate, Bloemfontein, November, 200 m a.g.l.

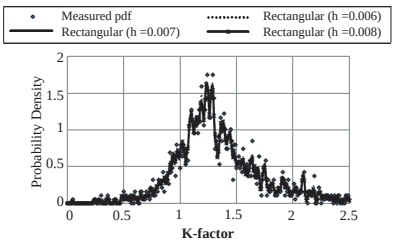

Figure 33. Rectangular kernel density estimate, Cape Town, February, 200 m a.g.l.

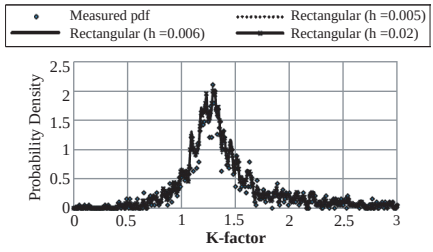

Figure 34. Rectangular kernel density estimate, Cape Town, May, 200 m a.g.l.

value at a given location. Local methods consider only a fixed number of samples within a certain search radius to the point being estimated. Global methods are known to produce smooth estimates but are very sensitive to outliers. On the other hand, local methods produce less smooth surfaces but are less sensitive to outliers. Global methods

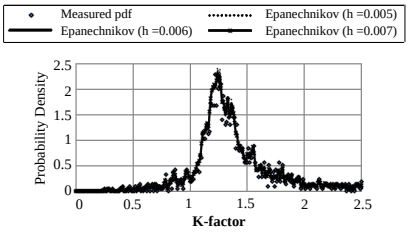

Figure 35. Epanechnikov kernel density estimate, Cape Town, August, 200 m a.g.l.

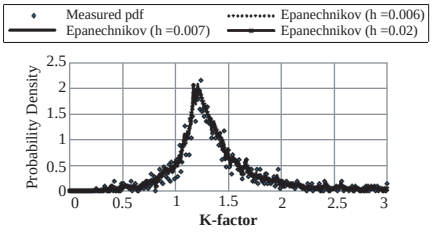

Figure 36. Epanechnikov kernel density estimate, Cape Town, November, 200 m a.g.l.

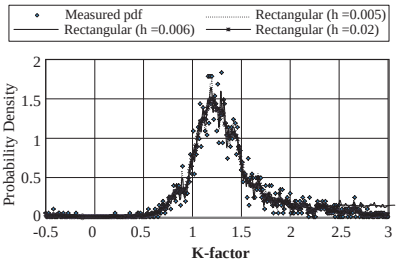

Figure 37. Rectangular kernel density estimate, Durban, February, 200 m a.g.l.

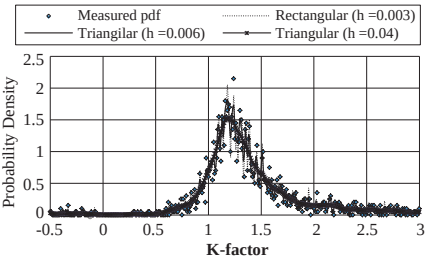

Figure 38. Triangular kernel density estimate, Durban, May, 200 m a.g.l.

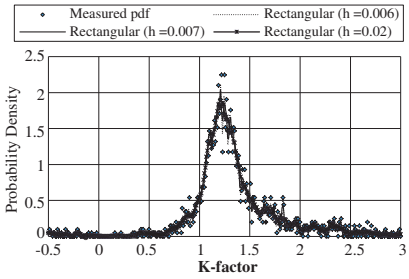

Figure 39. Rectangular kernel density estimate, Durban, August, 200 m a.g.l.

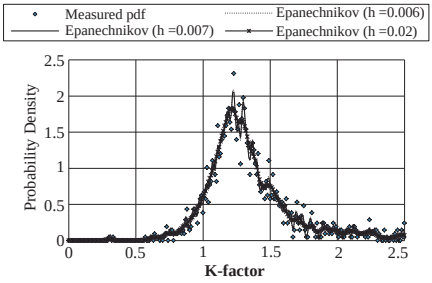

Figure 40. Epanechnikov kernel density estimate, Durban, November, 200 m a.g.l.

include trend surfaces, Fourier series and many others while local methods include Radial Basis Functions, Kriging and Inverse Distance Weighting (IDW) [33] among others.

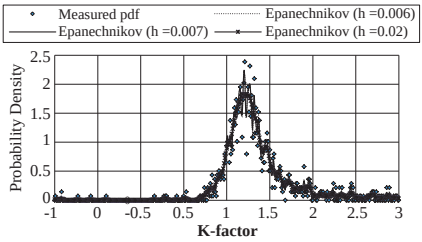

Figure 41. Epanechnikov kernel density estimate, Polokwane, February, 200 m a.g.l.

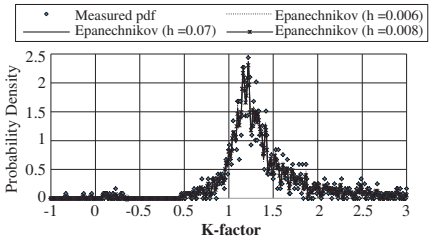

Figure 42. Epanechnikov kernel density estimate, Polokwane, May, 200 m a.g.l.

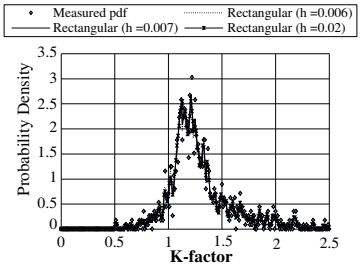

Figure 43. Rectangular kernel density estimate, Polokwane, August, 200 m a.g.l.

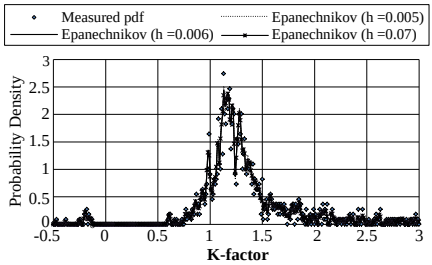

Figure 44. Epanechnikov kernel density estimate, Polokwane, November, 200 m a.g.l.

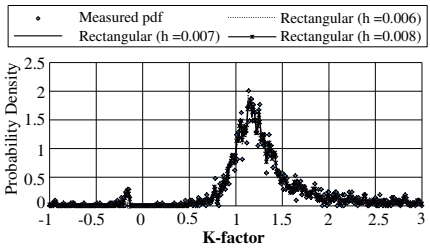

Figure 45. Rectangular kernel density estimate, Pretoria, February, 200 m a.g.l.

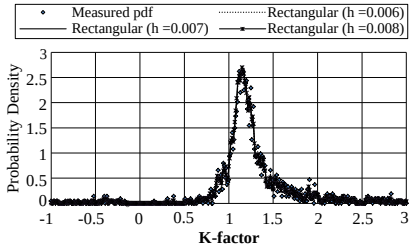

Figure 46. Rectangular kernel density estimate, Pretoria, May, 200 m a.g.l.

3.1. Inverse Distance Weighting (IDW)

IDW is a deterministic interpolation technique. This technique is based on the proposition that things that are closer are more alike than those farther apart. As such, IDW uses a weighting policy to

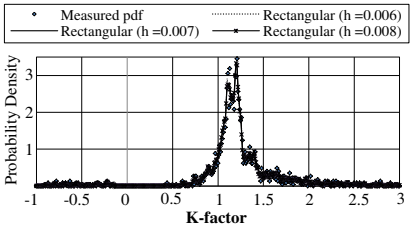

Figure 47. Rectangular kernel density estimate, Pretoria, August, 200 m a.g.l.

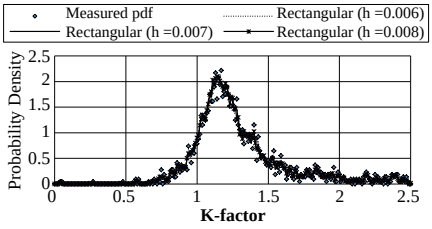

Figure 48. Rectangular kernel density estimate, Pretoria, November, 200 m a.g.l.

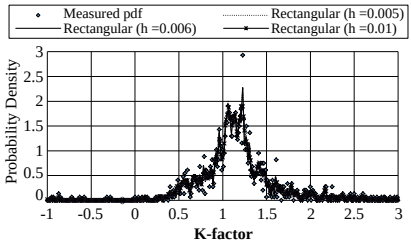

Figure 49. Rectangular kernel density estimate, Upington, February, 200 m a.g.l.

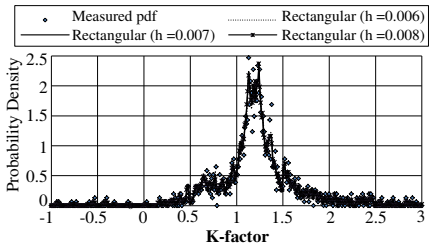

Figure 50. Rectangular kernel density estimate, Upington, May, 200 m a.g.l.

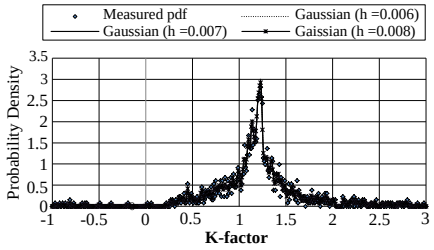

Figure 51. Gaussian kernel density estimate, Upington, August, 200 m a.g.l.

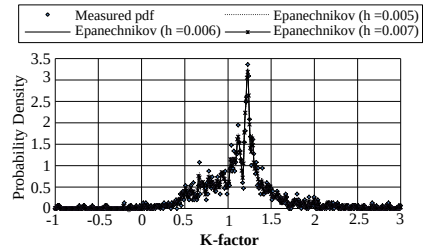

Figure 52. Epanechnikov kernel density estimate, Upington, November, 200 m a.g.l.

estimate values where data is not available with points that are closer to the prediction point assigned more weight than those farther from it [34]. The predicted estimate is then linear combination of the weighted measured values. The weight assignment in IDW is based on a power parameter, p that controls how much influence points have

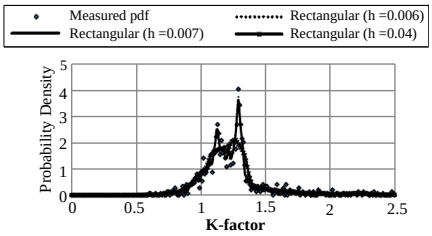

Figure 53. Rectangular kernel density estimate, Bethlehem, February, 200 m a.g.l.

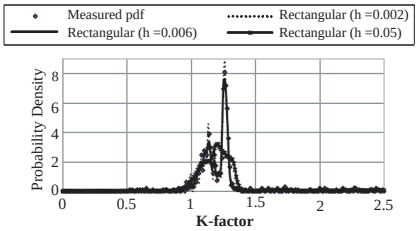

Figure 54. Rectangular kernel density estimate, Bethlehem, May, 200 m a.g.l.

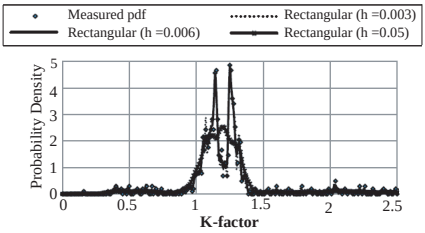

Figure 55. Rectangular kernel density estimate, Bethlehem, August, 200 m a.g.l.

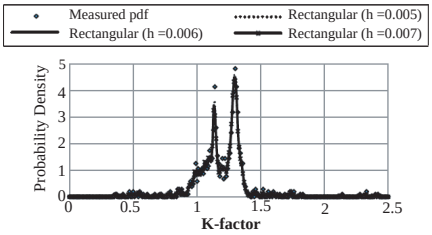

Figure 56. Rectangular kernel density estimate, Bethlehem, November, 200 m a.g.l.

on the predicted value. The higher the power parameter, the more the influence closer points have on the predicted value and vice versa. Typically, the power parameter is assigned value of 2 or 3 but the choice can also be made based on error measurement resulting in optimal IDW [35]. Mathematically, the IDW predictor is given by [35, 36]:

$$k\left(x,y\right)=\sum_{i=1}^{N}w_{i}k(x_{i},y_{i}) \tag{14}$$

where $k(x,\, y)$ is the value to be predicted, N is the number of sample points, $k(x_i,\, y_i)$ is the known value at sample point $(x_i,\, y_i)$ and w_i is the weight associated with it. The weight is given by [37]:

$$w_{i}=\frac{d_{i}^{-p}}{\sum_{i=1}^{N}d_{i}^{-p}} \tag{15}$$

where p is the power parameter, d is the Euclidian distance between the prediction point and the sample point and is given by [36] :

$$d=\sqrt{(x-x_{i})^{2}+(y-y_{i})^{2}} \tag{16}$$

where all parameters are as described in (14) and (15). The weighting in IDW is such that the sum of all the weights sum to unity [35]:

$$\sum_{i=1}^{N} w_i = 1 \tag{17}$$

Since IDW uses a simple weighting scheme, that is, it is based on the Euclidian distance between the interpolating point and the data points alone, the level of subjectivity is low hence computation speeds are faster compared to other sophisticated methods like kriging.

3.2. Kriging

Krigingis a stochastic interpolator but similar to IDW in that it also employs weighting to predict unknown values. Just as in IDW, the predicted value is a linear combination of the known weighted samples [32]. Points closer to the prediction point are also assigned more weight compared to those farther apart. However, the weighting used in kriging is more complex and involves spatial autocorrelation between the predicted point and known data points [37]. These spatial autocorrelation is modeled using the empirical semivariogram. The semivariogram is a plot of the semivariances against the separation distances (lag distances) of the known data points. The relationship that best describes the semivariogram is then used to build covariance matrices necessary for the determination of the weights. However, there are several known semivariogram models that can be fitted for the empirical semivariogram. They include the spherical, exponential, cubic, bessel, j-bessel and Gaussian and many others [33]. There are different kriging techniques; ordinary kriging, simple kriging, cokriging, kriging with trend and universal kriging [32]. The semivariance is a measure of the dissimilarity of a measured variable and is given by the average squared difference between the data values and is given by [37–40]:

$$\gamma(h) = \frac{1}{2N\,(h)} \sum\nolimits_{(i,j|h_{ij}=h)} (k_i - k_j)^2 \tag{18}$$

where $N(h)$ is the number of data values separated by a distance h.

Of these, ordinary kriging is the most commonly used and is the only one discussed further.

3.2.1. Ordinary Kriging

In ordinary kriging, the mean is assumed constant and unknown in the local neighbourhood of the prediction point. The kriging weights sum

to unity and are computed from [33, 40]:

$$\lambda_{ok} = Z_{ok}^{-1} M_{ok} \tag{19}$$

where λ_{ok} is the weights vector matrix, Z_{ok}^{-1} is the covariance matrix for the known data points and M_{ok} is the covariance vector matrix between the prediction data point and known data points. The kriging predictor is then given by [37, 40]:

$$k_{ok}^{*}(x, y) = \sum_{i=1}^{N} \lambda_{oki} k_{oki}(x_i, y_i) \tag{20}$$

where $k_{oki}(x_i, y_i)$ is the data value at point (x_i, y_i) and and λ_{oki} is the weight associated with it and N is as defined in (14). The seasonal measured values of the k-factor are gridded using PAST open source software [41] to create a smooth continuous surface (matrix). These matrices are then exported to MATLAB where contours are plotted. This procedure is repeated for four different kriging semivariogram models shown in Table 5 [40, 41] and then IDW interpolation is performed last. The Root Mean Square Error (RMSE) associated with each interpolation is computed and tabulated in Table 7. The Root Mean Square Error is given by [37]:

$$\text{RMSE} = \sqrt{\left(\frac{1}{N}\sum_{i=1}^{N}(k^{*} - k)^2\right)} \tag{21}$$

Table 5. Semivariogram models.

Model	Model equation
Cubic	$\gamma(h) = \begin{cases} c+S\cdot(7h^2-8.75h^3+3.75h^5-0.75h^7) & h\leq 1 \\ c+S & h\geq 1 \end{cases}$
Gaussian	$\gamma(h) = c + S\cdot\left(1-\exp\left(h^2\right)\right)$
Exponential	$\gamma(h) = c + S\cdot(1-\exp(-3h))$
Spherical	$\gamma(h) = \begin{cases} c + S\cdot\left(\frac{3}{2}h - \frac{1}{2}h^3\right) & h \leq 1 \\ c + S & h \geq 1 \end{cases}$

3.3. Interpolation Results and Discussion

The measured seasonal k-factor statistics are shown in Table 6. The interpolation RMSE errors are shown in Table 7. The kriging method that produces the best error performance and inverse distance weighting contour maps are the only ones presented due to space

Table 6. Measured median k-factor values.

Location	Latitude	Longitude	Month (Season)			
			February	May	August	November
Bloemfontein	29°06′S	26°18′E	1.24	1.21	1.21	1.22
Cape Town	33°59′S	18°36′E	1.26	1.29	1.30	1.27
Durban	29°58′S	30°57′E	1.28	1.26	1.26	1.26
Polokwane	23°54′S	29°28′E	1.27	1.27	1.23	1.23
Pretoria	25°55′S	28°13′E	1.22	1.19	1.19	1.20
Upington	28°24′S	21°16′E	1.14	1.20	1.19	1.16
Bethlehem	28°15′S	28°20′E	1.16	1.21	1.17	1.14

Table 7. Interpolation RMSE errors.

	Ordinary kriging semivariogram models				Inverse Distance weighting
	Spherical	Exponential	Gaussian	Cubic	
Feb.	0.0643	0.0645	0.205	0.0956	0.0456
May	0.0377	0.0416	0.080	0.0379	0.0335
Aug.	0.0374	0.0396	0.0908	0.0494	0.0329
Nov.	0.0560	0.0557	0.204	0.088	0.0399

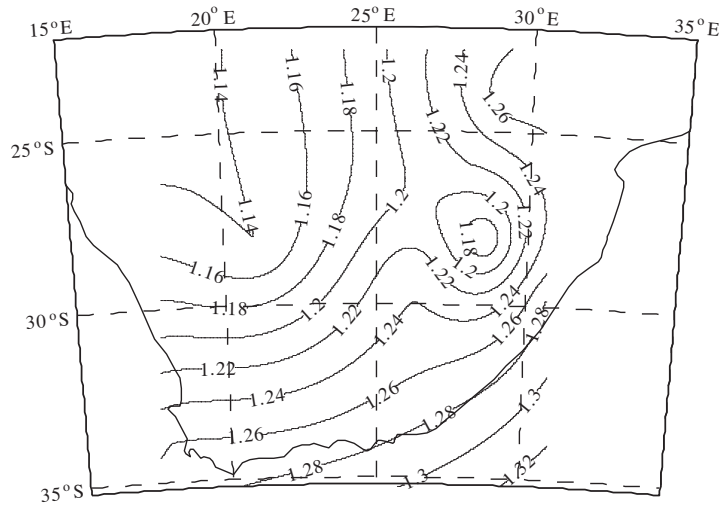

Figure 57. February kriging spherical semivariogram model median k-factor contours for South Africa.

considerations. These maps are shown in Figures 57–64. It is seen, from Table 7, that the spherical semivariogram model produces the best error performance in February, May and August while the exponential model is the best for November. The error performance for the IDW methodis very close to the best performing semivariogram

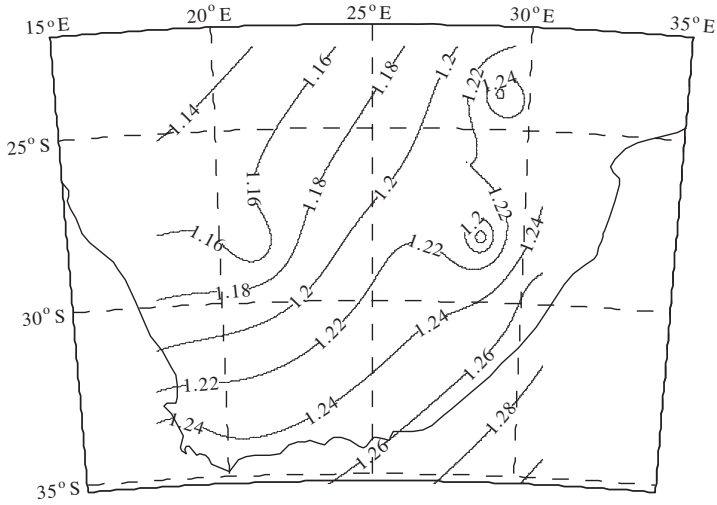

Figure 58. February IDW median k-factor contours for South Africa.

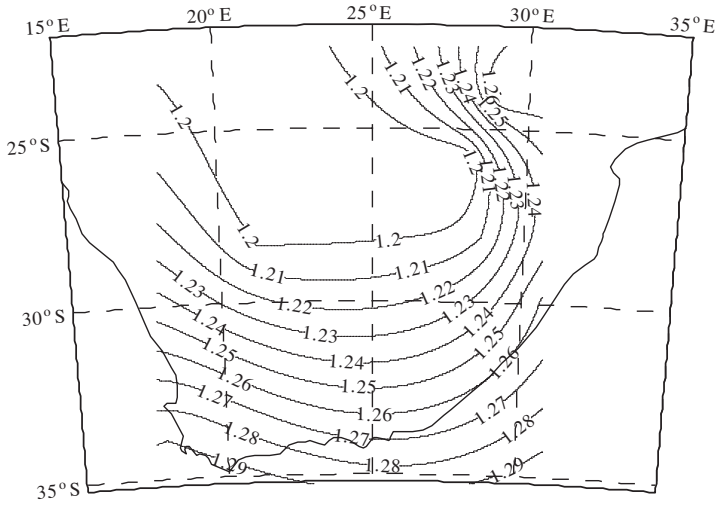

Figure 59. May kriging spherical semivariogram model median k-factor contours for South Africa.

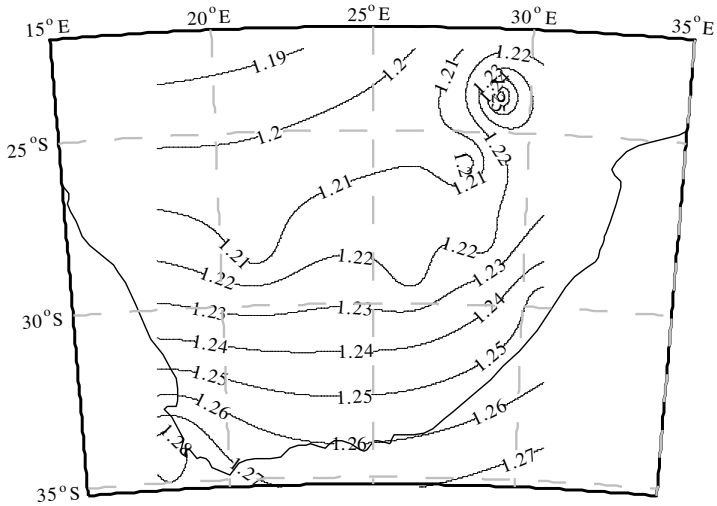

Figure 60. May IDW median k-factor contours for South Africa.

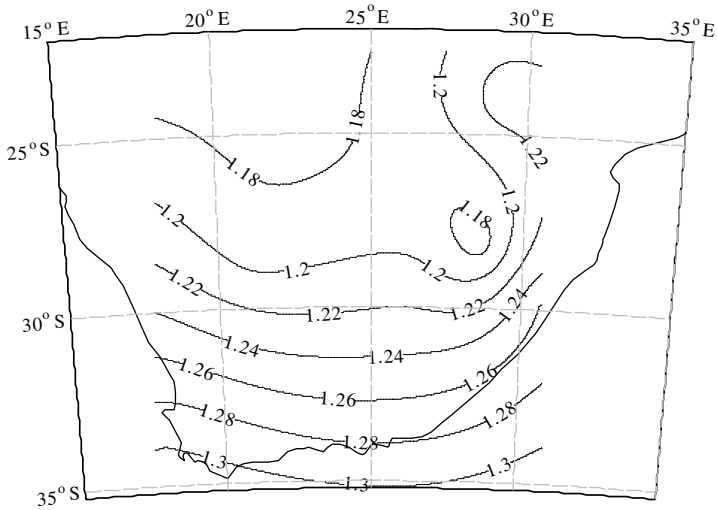

Figure 61. August kriging spherical semivariogram model median k-factor contours for South Africa.

model for each season. The largest difference in error performance is observed for February (0.0187) while the smallest is for May (0.0042). The Gaussian semivariogram model produces the worst error performance in all the four seasons. Overall, the IDW method produces

the least error in all the seasons and is most recommended for the seasonal interpolation of the k-factor in South Africa.

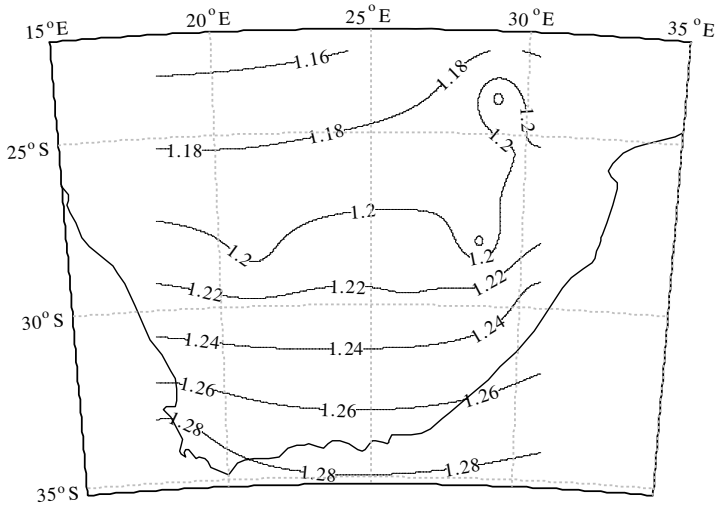

Figure 62. August IDW median k-factor contours for South Africa.

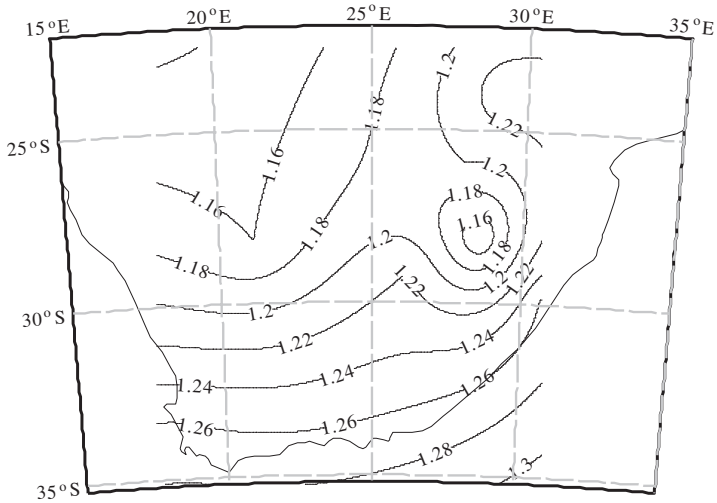

Figure 63. November kriging exponential semivariogram model median k-factor contours for South Africa.

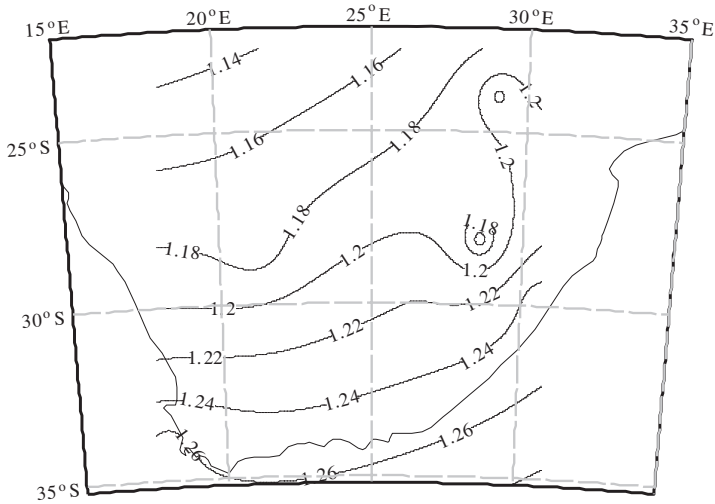

Figure 64. November IDW median k-factor contour plot.

4. CONCLUSION

The seasonal distribution and variation of the median k-factor for South Africa has been studied in this paper. Both parametric (curve fitting) and non-parametric (kernel density estimation) methods of density modeling have been used to formulate solutions of the k-factor distribution. Parametric methods impose restrictive assumptions about the data distribution and therefore may miss out on fine structures of the data distribution. By using certain parameters to define the data distribution, they may actually not follow the measured probability density function so much and thereby resulting in larger errors as can be seen with the curve fitting results in Table 1. The month of August produces the largest curve fitting errors for six of the seven locations, except in Polokwane where the worst performing month is November, while February produces the least error in all the seven locations. They are however easier to interpret since you can easily use parameters to summarize the data structure, for example, using the mean, median, standard deviation and variance, among others. The non-parametric technique used here is a better replacement for the traditional histograms used to represent data. Kernel methods have the advantage that they follow the measured pdf as much as possible and produce much smaller errors compared to parametric methods as can be seen from Table 4. The optimal choice of the smoothing parameter, h is key to achieving the best

kernel results. Overall, the rectangular kernel produces the best error performance for most of the seasons as can be seen in Table 4 and Figures 29–56 and is therefore the most recommended method for non-parametric modeling of the k-factor for South Africa. Also, all the four kernels used have a much superior error performance than the curve fitting method. From the distribution modeling results, we conclude that just as in [19, 21, 22], the distribution of the effective earth radius factor for South Africa is bell-shaped, centered almost symmetrically around a median value, μ_k. The interpolation of the seasonal k-factor measurements has been accomplished using four kriging semivariogram models and inverse distance weighting. The seasonal contour maps of the k-factor in South Africa have been produced for the four seasons of the year as spelt out under ITU-R recommendation P.453-12. The RMSE error performance in Table 7 shows that the IDW technique produces the least errors thus making it the most favorable. The spherical semivariogram model performs best in February, May and August and is therefore the recommended kriging method for the seasonal interpolation and mapping of the median k-factor statistics for South Africa. Results obtained in this paper will be critical for better and improved microwave and UHF link planning in South Africa as per the procedures outlined in ITU-R recommendation P.530-14 thereby addressing diffraction fading adequately.

ACKNOWLEDGMENT

The authors are grateful to the South African Weather Service (SAWS) for providing the radiosonde data measurements used in this paper.

REFERENCES

1. Cost 255 Final Report, "Radio wave propagation modelling for Satcom services at Ku-band and above," *European Space Agency*, SP-1252, March 2002.
2. Ayantunji, B. G., P. N. Okeke, and J. O. Urama, "Diurnal and seasonal variation of surface refractivity over Nigeria," *Progress in Electromagnetics Research B*, Vol. 30, 201–222, 2011.
3. Adenugba, D. A., "A Vb.Net class library and client application for radio refractivity," *International Journal of Computer Applications*, Vol. 33, No. 3, November 2011.
4. Asiyo, M. O. and T. J. Afullo, "Statistical estimation of fade depth and outage probability due to multipath propagation in South

Africa," *Progress In Electromagnetics Research B*, Vol. 46, 251–274, 2013.

5. Adediji, A. T. and M. O. Ajewole, "Vertical profile of the radio refractivity gradient in Akure, South-West Nigeria," *Progress In Electromagnetics Research C*, Vol. 4, 157–168, 2008.
6. Chaudhary, N. K., D. K. Trivedi, and R. Gupta, "The impact of k-factor on wireless link in Indian semi-desert terrain," *Int. J. Advanced Networking and Applications*, Vol. 2, No. 4, 776–779, 2011.
7. Nel, J. W., S. J. Erasmus, and S. Mare, "The establishment of a radio refractivity database for Southern Africa," *IEEE*, TH0219-6/88/0000-0144, 1988.
8. Ajayi, G. O., "Physics of the troposphere radio-propagation," *International Centre for Theoretical Physics, Internal Report No. IC/89/23*, Miramare, Trieste, Italy, February 1989.
9. Freeman, R. L., *Radio System Design for Telecommunications*, 3rd Edition, Wiley-Interscience, John Wiley & Sons Inc., New York, 2007.
10. Adediji, A. T., M. O. Ajewole, S. E. Falodun, and O. R. Oladosu, "Radio refractivity measurement at 150 m altitude on TV tower at Akure, South-West Nigeria," *Journal of Engineering and Applied Sciences*, Vol. 2, No. 8, 1308, 2007.
11. ITU-R, "The radio refractive index: Its formula and refractivity data," ITU-R Recommendation P.453-12, 2012.
12. Al-Ansari, K., A. A. Abdulhadi, and R. Kamel, "Statistical analysis of refractivity in UAE," *International Symposium on Rainfall Rate and Radio Wave Propagation*, 2007.
13. Palmer, A. J. and D. C. Baker, "Predicting the long-term average of the effective earth radius factor for South Africa using ground based observations," *SAIEE Africa Research Journal*, Vol. 97, No. 2, 182–185, June 2006.
14. Palmer, A. J., "A novel empirical model of the k-factor for radio propagation in Southern Africa for communication planning applications," Ph.D. Thesis, University of Pretoria, South Africa, November 2003.
15. Palmer, A. J. and D. C. Baker, "A novel semi-empirical model of the effective earth radius factor," *IEEE Transactions on Broadcasting*, Vol. 52, No. 4, 557–565, December 2006.
16. Serdega, D. and G. Ivanovs, "Refraction seasonal variation and that influence on to GHz range microwaves availability," *Electronics and Electrical Engineering*, Vol. 6, No. 78, ISSN 1392–

1215, 2007.

17. Parsons, J. D., *The Mobile Radio Propagation Channel*, John Wiley and Sons, ISBN 0-470-84152-4, 2000.
18. Adediji, A. T. and M. O. Ajewole, "Variation of radio refractivity and effective earth radius factor (k-factor) over Akure, South Western Nigeria," *IEEE*, 978-1-4244-5118-0/11, 2011.
19. Odedina, P. K. and T. J. Afullo, "On the k-factor distribution and diffraction fading for Southern Africa," *SAIEE Africa Research Journal*, Vol. 97, No. 2, June 2006.
20. ITU-R, "Propagation data and prediction methods required for the design of terrestrial line-of-sight systems," ITU-R Recommendation P.530-14, 2012.
21. Odedina, P. K. and T. J. Afullo, "Effective earth radius factor characterization for line-of-sight paths in Botswana," *IEEE AFRICON Proceedings*, 227–232, 2004.
22. Odedina, P. K. and T. J. Afullo, "Effective earth radius factor measurement and modeling for radio link design in Botswana," *SAIEE Africa Research Journal*, Vol. 99, No. 3, 2008.
23. Fulgence, D., "Effective earth radius distribution for Central Africa: Rwanda and north-western Tanzania," M.S. Thesis, National University of Rwanda, August 2012.
24. Silverman, B. W., *Density Estimation for Statistics and Data Analysis*, Chapman and Hall, London, 1986.
25. Sheather, S. J., "Density estimation," *Statistical Science*, Vol. 19, No. 4, 588–597, 2004.
26. Zucchini, W., "*Applied Smoothing Techniques, Part 1: Kernel Density Estimation*," October 2003.
27. Froehlich, D. F. and M. Rahman, "A note on the choice of the smoothing parameter in the kernel density estimate," *BRAC University Journal*, Vol. VI, No. 1, 59–68, 2009.
28. Sain, S. R., "Adaptive kernel density estimation," Ph.D. Thesis, Rice University, Houston, Texas, August 1994.
29. Faraway, J. J. and M. Jhun, "Bootstrap choice of bandwidth for density estimation," *American Statistical Association Journal,* Vol. 85, No. 412, 1990.
30. Raykar, V. C. and R. Duraiswami, "Very fast optimal bandwidth selection for univariate kernel density estimation," Perceptual Interfaces and Reality Laboratory of Maryland University, June 28, 2006.
31. Haithcoat, T., "Spatial interpolation," University of Missouri, Columbia, 1987.

32. Bohling, G., "Kriging," *Kansas Geological Survey*, C&PE 940, October 19, 2005.
33. Johnston, K., J. M. Hoef, K. Krivoruchko, and N. Lucas, "Using ArcGIS geostatistical analyst," *GIS by ESRI*, USA, 2001.
34. Odedina, P. K. and T. J. Afullo, "Use of spatial interpolation technique for the determination of the geoclimatic factor and fade calculation for South Africa," *Proceedings of IEEE AFRICON Conference*, Namibia, September 26–28, 2007.
35. Li, J. and A. D. Heap, "A review of spatial interpolation methods for environmental scientists," *Geoscience*, Record 2008/23, Australia, 2008.
36. Azpurua, M. and K. Dos Ramos, "A comparison of spatial interpolation methods for estimation of average electromagnetic field magnitude," *Progress In Electromagnetics Research M* Vol. 14, 135–145, 2010.
37. Bello-Pineda, J. and J. L. Hernandez-Stefanoni, "Comparing the performance of two interpolation methods for creating a digital bathymetric model of the Yucatan submerged platform," *Pan-American Journal of Applied Aquatic Sciences*, Vol. 2, No. 3, 247–254, 2007.
38. Boer, E. P. J, K. M. de Beurs, and A. W. Hartkamp, "Kriging and thin plate splines for mapping climatic variables," *International Journal of Applied Earth Observation and Geoinformation*, Vol. 3, No. 2, 146–154, 2001.
39. Janis, M. J. and S. M. Robeson, "Determining the spatial representativeness of air-temperature records using variogram-nugget series," *Physical Geography*, Vol. 25, No. 6, 513–530, 2004.
40. LeMay, Jr., N. E., "Variogram modeling and estimation," M.S. Thesis in Applied Mathematics, University of Colorado, Denver, 1998.
41. Hammer, O., *Paleontological Statistics Version 2.17 Reference Manual*, Natural History Museum, University of Oslo, 1999–2002.